Optimal Transient Control of In-Motion Wireless Power Transfer for Receiving Energy Maximization Using Envelope Model

Keiichiro Tokita[*a)] Student Member, Sakahisa Nagai[*] Member
Toshiyuki Fujita[*] Member, Hiroshi Fujimoto[*] Senior Member
Yoichi Hori[*] Fellow, Giuseppe Guidi[**] Non-member

In-motion wireless power transfer (WPT) is expected to solve many problems of electric vehicles (EVs). To transfer a large amount of energy to vehicles running at high speed, quick-start charging is needed. However, the sudden starting of the power transmission causes a large current overshoot, which damages the equipment of the WPT system. Therefore, it is commonly thought that the transient property of the current must be improved. However, the transient control method that considers both the current overshoot and the receiving energy is yet to be developed. Here, we propose a novel control method using the envelope model of the transient response. We apply the precise envelope model with d-q conversion to the starting of the power transmission considering the different modes of diodes. The proposed method successfully maximized the received energy while eliminating the current overshoot. This method is expected to be an essential technique for the practical use of in-motion WPT.

Keywords: wireless power transfer, transient property, envelope model, constant voltage load, energy maximization

1. Introduction

In recent years, wireless power transfer (WPT) has been widely studied. In particular, WPT using magnetic resonance coupling enables high-efficiency and high-power transmission even with a large air gap between a transmitting coil and a receiving coil [(1) (2)]. Therefore, it is expected to be used for many applications such as mobile devices, industrial machinery, and transportation [(3) (4)].

As a solution to environmental problems, the use of electric vehicles (EVs) is expected to increase instead of the internal combustion engine vehicles (ICEVs) worldwide in the future. However, current EVs have a serious problem in their shorter mileage per charge compared to ICEVs. As a technique to use WPT for EVs, in-motion wireless power transfer has been studied [(5) (6)]. This is a method of transmitting power wirelessly from the transmitting coil on roads to the receiving coil on the bottom of EVs. The authors also have developed in-motion WPT with the experimental EV in Fig. 1 [(7)]. In-motion WPT will not only solve the problem of short mileage per charge but also enable the large reduction of on-board batteries and the price down of EVs.

However, in-motion WPT has unique problems that do not matter in the previous WPT applications. Considering that the length of the transmitting coil is 1 m and that the vehicle runs on a highway at a speed of 100 km/h, the time of stay on a single transmitting coil is very short 36 ms. Therefore, fast vehicle detection and transmission start are required [(8)].

a) Correspondence to: tokita.keiichiro18@ae.k.u-tokyo.ac.jp
[*] The University of Tokyo
5-1-5, Kashiwanoha, Kashiwa, Chiba, 277-8561 Japan
[**] SINTEF Energy Research
Sem Sælands vei 11, 7034, Trondheim, Norway

Fig. 1. Experimental EV FPEV5 in our group [(7)].

To transmit a large amount of energy in a short time, the transmitting-side AC voltage must be quickly raised to a steady-state value after the vehicle detection. On the other hand, if the voltage is changed too rapidly, a large overshoot occurs as a transient response in the transmitting-side and receiving-side current [(9)]. The large current overshoot exceeding the rated value must be decreased because it can harm the equipment.

To control the transient response, many studies have been conducted to derive models of the transient response in various circuit topologies, such as the S-S (Series-Series) topology and the LCC topology [(10) (11)]. In particular, the paper [(12)] proposed an envelope model of the transient response in a WPT circuit for a constant-voltage load in an actual EV and succeeded in accurately describing the transient characteristics of the current waveform under varying voltage. By extending the current envelope model to the discontinuous current mode of diodes, a method to control the current transient response at the beginning of the power supply was proposed [(13)].

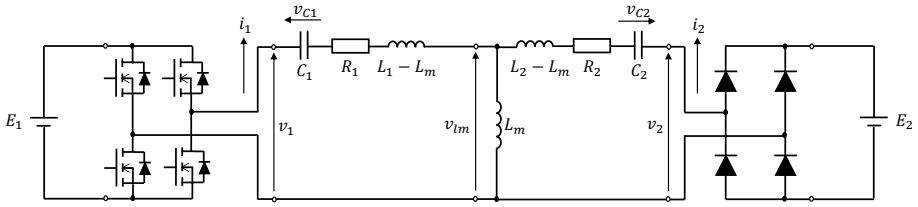

Fig. 2. S-S (Series-Series) compensation circuit with a receiving-side constant voltage load.

In the previous studies, the trajectory of the transmitting-side voltage which eliminates the transmitting-side current overshoot was proposed. However, the transient control method that considers both the current overshoot and the receiving energy is yet to be developed. Here, we propose a novel control method using the envelope model of the transient response. We apply the precise envelope model with d-q conversion to the starting of the power transmission considering the different modes of diodes. This paper aims to consider the problem of finding the transmitting-side voltage trajectory that maximizes the amount of receiving energy in the framework of optimization.

2. Envelope Modeling

2.1 S-S (Series-Series) compensation circuit It is difficult to control the instantaneous waveform of current or voltage because the frequency used in WPT is high. On the other hand, it gets easier to control the envelope waveform because it does not change as quickly as the instantaneous values. In this section, the envelope modeling is derived which describes the relationship between the voltage and the envelope of current [12].

As shown in Fig. 2, the equivalent circuit which has the Constant Voltage Load (CVL) on the receiving side is supposed to express the in-motion WPT circuit. Both the transmitting side and the receiving side adopt LC series circuits (S-S compensation circuit). E_1 is DC source voltage, and high-frequency AC voltage on the transmitting side v_1 is created by the inverter. In this section, every AC value of voltage or current is regarded as a purely sinusoidal waveform and higher harmonics are neglected unless otherwise mentioned. This approximation is valid because the WPT circuit via magnetic resonance has band-pass property and higher harmonics are not associated with the power transfer. By adjusting the pulse width of the inverter output voltage, the amplitude of the fundamental wave of the transmitting-side voltage $|v_1|$ is manipulated in the range of

$$0 \le |v_1| \le \frac{4E_1}{\pi}. \cdots\cdots (1)$$

2.2 phasor conversion and envelope model As explained in the introduction, not the instantaneous value but the envelope is focused on in the proposed model. The sinusoidal wave of the angular frequency ω, the initial phase ϕ, and the time-variant amplitude $A(t)$ is expressed as :

$$\begin{aligned} x(t) &= A(t) \cdot \cos(\omega \cdot t + \phi) \\ &= \mathrm{Re}\left(A(t) \cdot e^{j\phi} \cdot e^{j\omega t}\right) \\ &= \mathrm{Re}\left\{\left(x_d(t) + jx_q(t)\right) \cdot e^{j\omega t}\right\}, \cdots\cdots (2) \end{aligned}$$

and the AC functions like current or voltage above is converted to the cartesian coordinates as

$$X(t) = x_d(t) + jx_q(t). \cdots\cdots (3)$$

The circuit equations of Fig. 2 are expressed as simultaneous equations with four variables : transmitting-side current i_1, receiving-side current i_2, transmitting-side capacitor voltage v_{C1}, receiving-side capacitor voltage v_{C2}, transmitting-side voltage v_1, and receiving-side voltage v_2. By the phasor conversion, the state equation with 6-dimensional state variable $\boldsymbol{x}$ and 2-dimensional input variable $\boldsymbol{u}$ are derived as follows :

$$\dot{\boldsymbol{x}} = \boldsymbol{A}\boldsymbol{x} + \boldsymbol{B}\boldsymbol{u} \cdots\cdots (4)$$

$$\boldsymbol{x} = [i_{1d} \;\; i_{2q} \;\; v_{C1d} \;\; v_{C1q} \;\; v_{C2d} \;\; v_{C2q}]^T \cdots\cdots (5)$$

$$\boldsymbol{u} = [|v_1| \;\; |v_2|]^T. \cdots\cdots (6)$$

In the phasor modeling, the direction of the d-axis is determined with reference to the transmitting-side voltage v_1. In this condition, the q component of transmitting-side voltage v_{1q} and the d component of receiving-side voltage v_{2d} are 0. In addition, i_{1q} and i_{2d} are almost zero so these values can be eliminated from the state variable. Therefore, the system can be regarded as a two-input system of the voltage amplitude as shown in (4) and (6).

For thinking about the diode modes, $v_{2,act}(t)$ is defined as the actual value of receiving-side AC voltage including higher harmonics. According to the value, this circuit has two types of modes :

mode 1) $|v_{2,act}(t)|$ is always lower than the battery voltage E_2 during a period, and the receiving-side rectifier does not conduct at all.

mode 2) $|v_{2,act}(t)|$ reaches the battery voltage E_2 during a period, and the receiving-side rectifier conducts on and off.

The different non-linear state-space model is derived for each mode. The mode 1) is discussed in the subsection 2.3 and the mode 2) in the subsection 2.4.

2.3 State equations when the rectifier does not conduct When $|v_{2,act}(t)|$ is always lower than the battery voltage E_2 during a period, the receiving-side rectifier does not conduct and the receiving side is open. In this mode, the voltage on the mutual inductance $v_{lm}(t)$ equals $v_{2,act}(t)$. The circuit equations are expressed as simultaneous equations with four variables:

$$L_1 \frac{di_1}{dt} = -R_1 i_1 - v_{C1} + v_1 \cdots\cdots (7)$$

$$C_1 \frac{dv_{C1}}{dt} = i_1 \cdots\cdots (8)$$

$$i_2 = 0 \cdots\cdots (9)$$

$$v_{C2} = 0 \cdots\cdots (10)$$

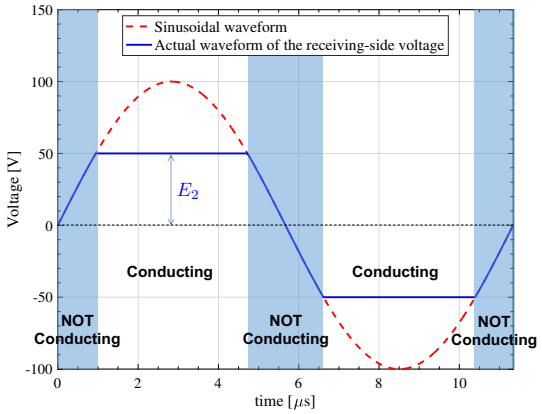

Fig. 3. The waveform of the receiving-side AC voltage when the diode rectifier conducts.

The d-q conversion mentioned in subsection 2.2 is applied to each instantaneous value. According to (7)-(10), the state equation with 6-dimensional state variable $\boldsymbol{x}$ and 2-dimensional input variable $\boldsymbol{u}$ is given as follows :

$$\dot{\boldsymbol{x}} = \boldsymbol{A_1}\boldsymbol{x} + \boldsymbol{B_1}\boldsymbol{u}. \cdots (11)$$

Each matrix is shown in (12) and (13):

$$\boldsymbol{A_1} = \begin{pmatrix} -\frac{R_1}{L_1} & 0 & -\frac{1}{L_1} & 0 & 0 & 0 \\ 0 & 0 & 0 & 0 & 0 & 0 \\ \frac{1}{C_1} & 0 & 0 & \omega & 0 & 0 \\ 0 & 0 & -\omega & 0 & 0 & 0 \\ 0 & 0 & 0 & 0 & 0 & 0 \\ 0 & 0 & 0 & 0 & 0 & 0 \end{pmatrix} \cdots (12)$$

$$\boldsymbol{B_1} = \begin{pmatrix} \frac{1}{L_1} & 0 & 0 & 0 & 0 & 0 \\ 0 & 0 & 0 & 0 & 0 & 0 \end{pmatrix}^T \cdots (13)$$

2.4 State equations when the rectifier conducts

When $|v_{2,act}(t)|$ reaches the battery voltage E_2 during a period, $|v_{2,act}(t)|$ is limited not to overcome the battery voltage E_2. In this condition, the waveform of $v_{2,act}(t)$ becomes the shape of blue line in Fig. 3. When $|v_{2,act}(t)|$ is lower than E_2, the waveform varies according to a sinusoidal wave (blue-background area in Fig. 3). However, the waveform is limited to $\pm E_2$ when $|v_{2,act}(t)|$ reaches E_2 (white-background area in Fig. 3). If the amplitude of sinusoidal wave (red line in Fig. 3) is very large, the waveform of $v_{2,act}(t)$ can be approximated by a rectangular wave.

The circuit equations are expressed as simultaneous equations with four variables:

$$L_{\sigma 1}\frac{di_1}{dt} = -R_1 i_1 + \frac{L_m R_2}{L_2} i_2 - v_{C1} + \frac{L_m}{L_2} v_{C2} + v_1 - \frac{L_m}{L_2} v_2 \quad (14)$$

$$L_{\sigma 2}\frac{di_2}{dt} = \frac{L_m R_1}{L_1} i_1 - R_2 i_2 + \frac{L_m}{L_1} v_{C1} - v_{C2} - \frac{L_m}{L_1} v_1 + v_2 \cdots (15)$$

$$C_1\frac{dv_{C1}}{dt} = i_1 \cdots (16)$$

$$C_2\frac{dv_{C2}}{dt} = i_2 \cdots (17)$$

$L_{\sigma 1}$ and $L_{\sigma 2}$ above are defined as follows:

$$L_{\sigma 1} = L_1 - \frac{L_m^2}{L_2} \cdots (18)$$

$$L_{\sigma 2} = L_2 - \frac{L_m^2}{L_1} \cdots (19)$$

The d-q conversion mentioned in the subsection 2.2 is applied to (14)-(17) as well as the subsection 2.3. CVL and a rectifier have two properties as follows:

(1) The phase difference between receiving-side voltage v_2 and receiving-side current i_2 is 180 degree (opposite phase).

(2) The amplitude of receiving-side voltage $|v_2|$ is determined as a function of the amplitude of transmitting-side voltage $|v_1|$ and battery voltage E_2.

Due to the first property, v_{2d} and v_{2q} are derived as follows:

$$v_{2d} = -|v_2| \cdot \frac{i_{2d}}{\sqrt{i_{2d}^2 + i_{2q}^2}} \simeq 0 \cdots (20)$$

$$v_{2q} = -|v_2| \cdot \frac{i_{2q}}{\sqrt{i_{2d}^2 + i_{2q}^2}} \simeq |v_2|. \cdots (21)$$

The approximation is valid for the reason explained in the subsection 2.2.

Eq. (14)-(17) are expressed as the state equation with 6-dimensional state variable $\boldsymbol{x}$ and 2-dimensional input variable $\boldsymbol{u}$ as follows :

$$\dot{\boldsymbol{x}} = \boldsymbol{A_2}\boldsymbol{x} + \boldsymbol{B_2}\boldsymbol{u}. \cdots (22)$$

Each matrix is shown in (23) and (24):

$$\boldsymbol{A_2} = \begin{pmatrix} -\frac{R_1}{L_{\sigma 1}} & 0 & -\frac{1}{L_{\sigma 1}} & 0 & \frac{L_m}{L_{\sigma 1} L_2} & 0 \\ 0 & -\frac{R_2}{L_{\sigma 2}} & 0 & \frac{L_m}{L_{\sigma 2} L_1} & 0 & -\frac{1}{L_{\sigma 2}} \\ \frac{1}{C_1} & 0 & 0 & \omega & 0 & 0 \\ 0 & 0 & -\omega & 0 & 0 & 0 \\ 0 & 0 & 0 & 0 & 0 & \omega \\ 0 & \frac{1}{C_2} & 0 & 0 & -\omega & 0 \end{pmatrix} (23)$$

$$\boldsymbol{B_2} = \begin{pmatrix} \frac{1}{L_{\sigma 1}} & 0 & 0 & 0 & 0 & 0 \\ 0 & \frac{1}{L_{\sigma_2}} & 0 & 0 & 0 & 0 \end{pmatrix}^T \cdots (24)$$

2.5 Condition of the diode mode change

The mode change from the non-conducting mode in the subsection 2.3 to the conducting mode in the subsection 2.4 is derived. The change occurs when

$$v_{lm}(t) = v_{2,act}(t) = E_2. \cdots (25)$$

At this moment, the rectifier begins to work.

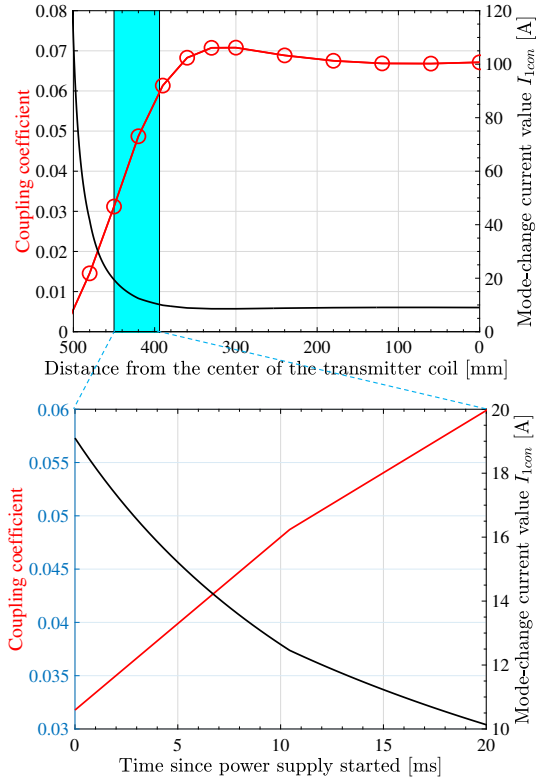

Fig. 4. The coupling coefficient k and the mode-change current value I_{1con} are expressed as the function of the receiving coil position as shown in the upper figure. The power supply is started at the position where the coupling coefficient becomes higher than 0.031. If the vehicle speed is 10 km/h, the coupling coefficient and the mode-change current value can be derived as the time function in the lower figure.

The phasor conversion mentioned in the subsection 2.2 is applied to $v_{lm}(t)$ and expressed in the phasor as follows:

$$V_{lm} = v_{lmd} + jv_{lmq}. \cdots (26)$$

Because $v_{lm}(t)$ is expressed as

$$v_{lm}(t) = L_m \frac{di_1(t)}{dt}, \cdots (27)$$

the amplitude $|V_{lm}|$ is derived as follows:

$$\begin{aligned} |V_{lm}| &= \left|v_{lmd} + jv_{lmq}\right| \\ &= \left|\frac{di_{1d}}{dt} + j\omega L_m i_{1d}\right| \cdots (28) \\ &\simeq \omega L_m i_{1d}. \cdots (29) \end{aligned}$$

By (25) and (29), the mode change occurs when

$$\omega L_m i_{1d} = E_2 \cdots (30)$$

$$\Leftrightarrow i_{1d} = \frac{E_2}{\omega L_m}. \cdots (31)$$

The i_{1d} value which satisfies (31) is defined as the mode-change current value I_{1con}. Because L_m is determined by the coil position, I_{1con} is also determined if the coil position when the diode mode change occurs is determined. Fig. 4 shows their relationship. By using this, the dynamics before and after the mode change is discussed in the next section.

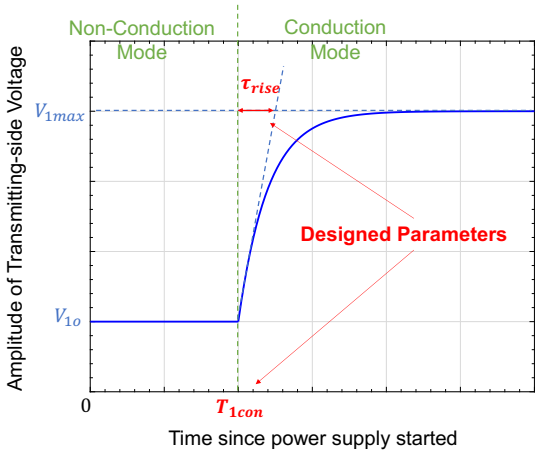

Fig. 5. Outline of the trajectory of the transmitting-side voltage amplitude.

3. Energy Maximization

3.1 Receiving Energy The receiving energy W is defined as follows:

$$W = \int_0^{T_f} E_2|i_2|dt \cdots (32)$$

$$\simeq \int_0^{T_f} [0 \quad -E_2 \quad 0 \quad 0 \quad 0 \quad 0]\,\boldsymbol{x}(t)dt \cdots (33)$$

$$= \int_{T_{con}}^{T_f} [0 \quad -E_2 \quad 0 \quad 0 \quad 0 \quad 0]\,\boldsymbol{x}(t)dt, \cdots (34)$$

where time $t = 0$ and $t = T_f$ are the start and the end time of charging, respectively. $t = T_{con}$ is the time of the diode mode change mentioned in the section 2. The conversion from (32) to (33) is valid because of the same reason with (20) and (21). The conversion from (33) to (34) is valid because the receiving-side current is kept at 0 during the diode rectifier is in the non-conduction mode.

3.2 Optimization Algorithm In this paper, many input trajectories are examined and the input voltage trajectory which realizes the most receiving energy is derived. By considering many patterns of input trajectories on both before and after the diode conduction separately, the best trajectory is derived. In creating the input voltage patterns, the following constraints are imposed:

(1) Before the diode conduction, the input voltage is kept constant at V_{1o}. The voltage value is automatically determined by the time of the diode mode change T_{con}.

(2) After the diode conduction, the input voltage is raised to the maximum voltage V_{1max}. The trajectory is assumed to be a response of a first-order delay system whose time constant is τ_{rise}.

The overview is shown in Fig. 5. The designed parameters are T_{con} and τ_{rise}. If T_{con} is determined once, I_{1con} and V_{1o} are automatically determined by Fig. 4.

4. Simulation

To verify the feasibility of the proposed method, the simulation using MATLAB/Simulink was conducted. The circuit

Table 1. Parameters in the simulation and experiment

Parameter	Value
Operating frequency f_0	86 kHz
Transmitter inductance L_1	245.7 µH
Transmitter resistance R_1	108.6 mΩ
Receiver inductance L_2	96.89 µH
Receiver resistance R_2	25.25 mΩ
Velocity of the vehicle	10 km/h
Transmitting-side DC-link voltage E_1	50 V
Receiving-side DC-link voltage E_2	50 V
Amplitude of transmitting-side AC voltage $\|v_1\|$	0 V → 50 V
Transmitting-side current Limit I_{1lim}	25.4 A
Receiving-side current Limit I_{2lim}	25.4 A
Coupling coefficient k	0.031 → 0.070 → 0.031
Whole charging time	324 ms
Control period of transmitting-side inverter	100 µs

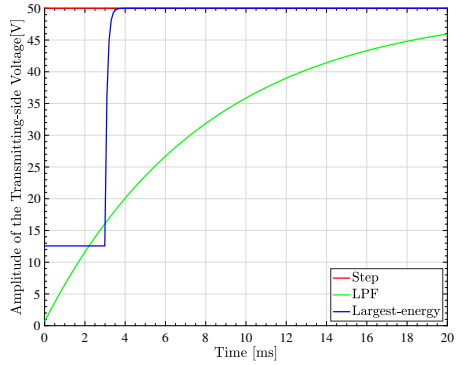

(a) Transmitting-side Input Voltage

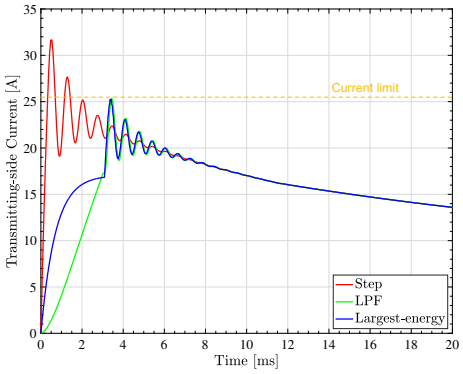

(b) Transmitting-side Current Envelope

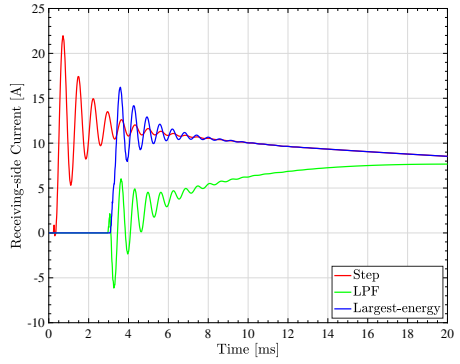

(c) Receiving-side Current Envelope

Fig. 6. Simulation results using the envelope model.

parameters are based on the experimental vehicle in Fig. 1, which are shown in Table 1.

In the simulation, T_{con} was changed in the range from 0 ms to 10 ms, in 0.1 ms increments. τ_{rise} was also changed in the range from 0 ms to 10 ms, in 0.1 ms increments. In total, $101 \times 101 = 10,201$ patterns of the input voltage trajectory were examined.

Some examples of the input voltage trajectory are shown in Fig. 6(a) and the corresponding transmitting-side / receiving-side current envelope waveforms are shown in Fig. 6(b) and Fig. 6(c), respectively. The receiving energy amount in the whole charging time (345.6 ms) is shown in Table 2. The input trajectory which realizes the most receiving energy in the current limit (blue line) was obtained. Compared to the best LPF trajectory, the receiving energy amount is almost 3 % larger in the proposed method. The percentage of the energy increase is expected if the vehicle speed is faster and the charging time is shorter.

The additional simulation verification was conducted for the largest-energy input trajectory. Fig. 7 shows the comparison between the model-based envelope line and the instantaneous waveform calculated by the circuit simulation. It is confirmed that the envelope is very accurate. Because the circuit simulation takes much more time than the calculation of the envelope model, trying a lot of input trajectories becomes

Table 2. Receiving energy of each case. When the trajectory violates the current limit, the receiving energy is expressed as "-" because the charging is impossible.

Notes	T_{con} [ms]	τ_{rise} [ms]	Receiving energy [J]
Step Trajectory	0	0	-
LPF Trajectory	0	7.5	122.079
Largest-energy Trajectory	2.9	0.1	125.505

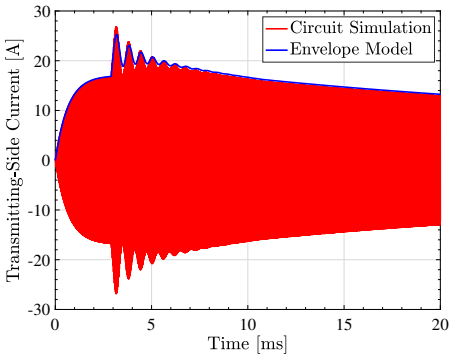

(a) Transmitting-side current

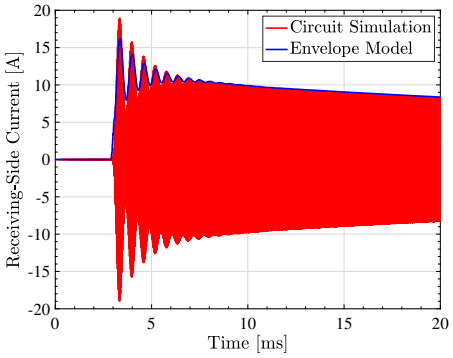

(b) Receiving-side current

Fig. 7. Simulation result of the receiving-side current for the largest-energy input trajectory. By the circuit simulation, the envelope was confirmed to be accurate.

Fig. 8. Experimental setup : In-motion WPT bench. The bench has a moving belt and the receiving coil is put on the bottom of the belt. The transmitting coil is fixed on the ground.

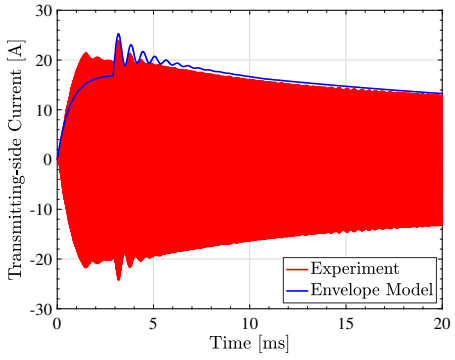

(a) Transmitting-side Current

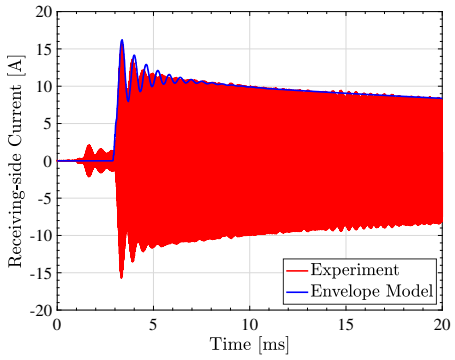

(b) Receiving-side Current

Fig. 9. Experimental result of the receiving-side current for the largest-energy input trajectory.

possible using the envelope model explained in the section 2.

5. Experiment

The in-motion WPT bench is used as the experimental setup, as shown in Fig. 8. The bench has a moving belt and the receiving coil is put on the bottom of the belt. The transmitting coil is fixed on the ground. By driving the servo motor attached to the belt, the coupling variation during the in-motion charging is realized.

Because it is difficult to measure power during the transient state, the receiving-side current was measured and compared to the simulation results. Fig. 9 shows the receiving-side current corresponding to Fig. 7. Waveforms similar to the simulation were observed. The error between the simulation and the experiment is thought to be attributed to the parameter misalignment, especially the imperfect resonance.

6. Conclusion

In this paper, a novel method of increasing the receiving energy using the precise envelope model of the circuit and the current limit information was proposed. By considering many patterns of input trajectories on both before and after the diode conduction separately, the best trajectory was derived. Using the simulation and the experiment, the feasibility of the proposed method was confirmed.

Acknowledgment

The contributions of Toyo Denki Seizo K.K. and NSK Ltd. are gratefully acknowledged. This work was partly supported by JSPS KAKENHI Grant Number 18H03768, JST CREST Grant Number JPMJCR15K3, JST-Mirai Program Grant Number JPMJMI17EM, and JST SICORP Grant Number JPMJSC17C4 (CONCERT-Japan), Japan.

References

(1) A. Kurs, A. Karalis, R. Moffatt, J. D. Joannopoulos, P. Fisher, and M. Soljacic, "Wireless Power Transfer via Strongly Coupled Magnetic Resonances," *Science*, vol. 317, no. 5834, pp. 83–86, jul 2007.

(2) K. Kusaka, K. Furukawa, and J. Itoh, "Development of Three-Phase Wireless Power Transfer System with Reduced Radiation Noise," *IEEJ Journal of Industry Applications*, vol. 8, no. 4, pp. 600–607, jul 2019.

(3) K. Hwang, J. Cho, J. Park, D. Har, and S. Ahn, "Ferrite Position Identification System Operating with Wireless Power Transfer for Intelligent Train Position Detection," *IEEE Transactions on Intelligent Transportation Systems*, vol. 20, no. 1, pp. 374–382, 2019.

(4) V. Doan, H. Fujimoto, T. Koseki, T. Yasuda, H. Kishi, and T. Fujita, "Simultaneous Optimization of Speed Profile and Allocation of Wireless Power Transfer System for Autonomous Driving Electric Vehicles," *IEEJ Journal of Industry Applications*, vol. 7, no. 2, pp. 189–201, 2018.

(5) D. Patil, M. K. McDonough, J. M. Miller, B. Fahimi, and P. T. Balsara, "Wireless Power Transfer for Vehicular Applications: Overview and Challenges," *IEEE Transactions on Transportation Electrification*, vol. 4, no. 1, pp. 3–37, mar 2018.

(6) S. Li and C. C. Mi, "Wireless Power Transfer for Electric Vehicle Applications," *IEEE Journal of Emerging and Selected Topics in Power Electronics*, vol. 3, no. 1, pp. 4–17, mar 2015.

(7) H. Fujimoto, O. Shimizu, S. Nagai, and T. Fujita, "Development of Wireless In-wheel Motors for Dynamic Charging -from 2nd to 3rd generation-," 2020.

(8) D. Kobayashi, K. Hata, T. Imura, H. Fujimoto, and Y. Hori, "Sensorless Vehicle Detection Using Voltage Pulses in Dynamic Wireless Power Transfer System," *EVS29 Symposium*, 2016.

(9) K. Hata, T. Imura, H. Fujimoto, and Y. Hori, "Soft-Start Control Method for In-motion Charging of Electric Vehicles Based on Transient Analysis of Wireless Power Transfer System," in *2018 IEEE Energy Conversion Congress and Exposition (ECCE)*. IEEE, sep 2018, pp. 2009–2015.

(10) A. Ong, P. K. S. Jayathurathnage, J. H. Cheong, and W. L. Goh, "Transmitter Pulsation Control for Dynamic Wireless Power Transfer Systems," *IEEE Transactions on Transportation Electrification*, vol. 3, no. 2, pp. 418–426, jun 2017.

(11) Y. Guo, L. Wang, Q. Zhu, C. Liao, and F. Li, "Switch-On Modeling and Analysis of Dynamic Wireless Charging System Used for Electric Vehicles," *IEEE Transactions on Industrial Electronics*, vol. 63, no. 10, pp. 6568–6579, oct 2016.

(12) G. Guidi and J. A. Suul, "Modelling techniques for designing high-performance on-road dynamic charging systems for electric vehicles," *EVS 31 & EVTeC 2018*, 2018.

(13) K. Tokita, H. Fujimoto, and Y. Hori, "Feedforward Transient Control for In-Motion Wireless Power Transfer Using Envelope Model," in *Proceedings - 2020 IEEE MTT-S Wireless Power Transfer Conference, WPTC2020*, 2020.